IR Imaging of Microsystems: special requirements, experiments and applications

K.-P. Möllmann, M. Vollmer
Brandenburg University of Applied Sciences
Microsystem and Optical Technologies
Magdeburger Straße 50
14770 Brandenburg
Germany

Abstract

For a lot of microsystems a uniform temperature or a spatial temperature distribution as well as thermal response time are among the most important parameters. Any contact probe for temperature measurement would induce appreciable thermal losses due to thermal conduction which either complicates the analysis or even makes it impossible. Therefore a contactless measurement is needed to analyze these parameters for microsystem components (e.g. reactors, sensors, actuators). Obviously IR imaging can play an important role for the thermal characterization of different microsystems, to support the research and development work, and to control the system operation without modifying the system performance [1,2]. In the past investigation of systems characterized by small dimensions in the µm-range and short time constants in the ms-range could only be studied by imaging devices operating in the visible spectral range. Today high-end thermal imaging cameras as the FLIR SC 6000 with frame rates up to some 36 kHz, temperature resolutions better than 20 mK and spatial resolutions better than 10 µm using high quality infrared optics are available. Such cameras offer the possibility to extend the investigations of microsystems to thermal imaging.
IR imaging of microsystems poses a number of problems which are usually not encountered when studying macroscopic objects [3]. We will first outline specific requirements concerning suppression of mechanical instabilities and vibrations, the need for close-up lenses or microscope objectives and the possibility of high speed recording. Second the improved characterization of fast energy transfer processes producing or consuming thermal energy in such miniaturized systems will be demonstrated.

Special requirements for IR imaging of Microsystems

- **Mechanical stability of set up**

Due to the small size of the microstructures a very stable mechanical construction of a test bench is necessary to avoid effects of mechanical instabilities or mechanical vibrations on the thermal imaging results. A breadboard or even better a vibration insulated optical table with adjustable sample and camera holders are well-suited for the microscopic thermal imaging analysis, see Fig. 1.

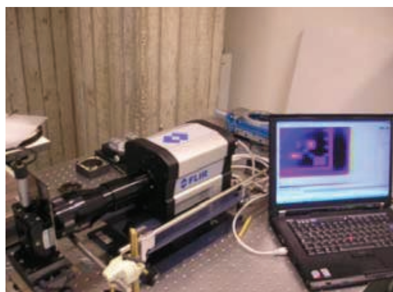

Fig. 1.: Experimental setup for microscopic thermal imaging using an optical table

- **Microscope objectives, close-up lenses, extender rings**

Usually a spatial resolution of thermal imaging much better than 1 mm is necessary although in practice the requirement depends on the microstructure size. IR cameras with a standard objective allowing spatial resolutions around 1 mm must be equipped with an additional close-up lens to increase the spatial resolution. For cameras with exchangeable lenses, extender rings can be used. The best spatial resolution is achieved by using a microscope optics. Fig. 2 demonstrates the improvement of the optical resolution for a miniaturized thermal emitter in a transistor housing using different components. The use of additional optical components for increasing the spatial resolution of the imaging is accompanied by a decreasing working distance (camera objective to object). Therefore the influence of the Narcissus-effect for non-black objects has to be considered [3].
Before analyzing temperatures at microscopic structures the spatial resolution of the equipment used needs to be determined to avoid temperature measurement errors. For the determination of the spatial resolution, chromium structures with a well defined size on a photolithography mask with a glass substrate can e.g. used. The mask should be heated up and the emissivity contrast of the mask can be used for the measurement. Fig. 3 depicts a measurement across a 34 µm line on the mask. Compared to the visible microscope image (Fig. 3 left, top) the thermogram appears blurred (Fig. 3 left, bottom).

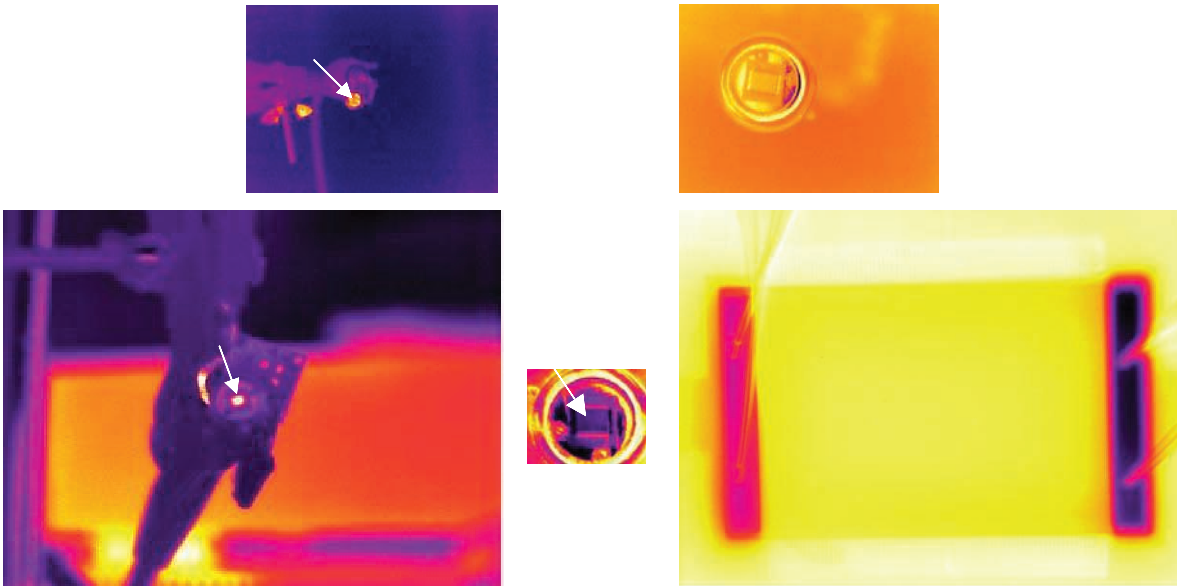

Fig. 2: Thermograms of a miniaturized infrared emitter (size 2.1 mm x 1.8 mm) in TO-39 housing. Region of interest as indicated by arrows in left and middle thermograms is shown expanded in the right images.
top: MW camera FLIR THV 550 (320 x 240 pixels) with a 24° optics (top, left) and an additional close-up lens (top, right)
bottom: MW camera FLIR SC6000 (640 x 512 pixels) with a 25 mm lens (bottom, left), additional extender ring (bottom, middle with 160 x 120 pixels) and microscope optics (bottom, right)

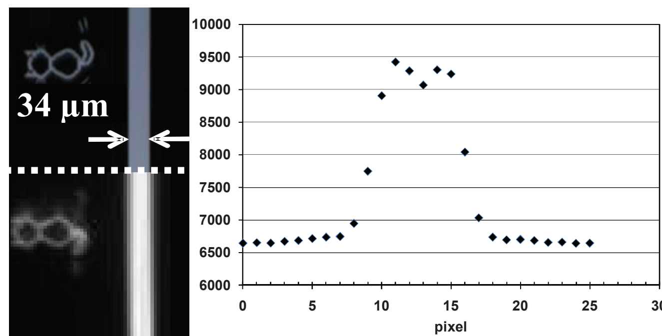

Fig. 3: VIS microscope image (top, left) and thermogram (bottom, left) of a line with a width of 34 µm on a chromium mask. Raw signal profile of the line measured in the thermogram (right) using the FLIR SC6000 camera

Raw signal data across the line were analyzed and a signal plateau was formed by about 6 pixels (Fig. 3, right). If this number of pixels is compared to the line width of 34 µm one may conclude for this camera equipment that resolution per pixel amounts to around 5 – 6 µm.

- **High speed recording**

Thermal processes as heat transfer and temperature changes in microsystems are mostly characterized by low time constants in the ms to µs range due to the low heat capacitance or thermal mass. For time resolved thermal imaging high-speed data acquisition is necessary. The limitation of the time resolution is given by the response time of the IR camera. For cameras with photon detectors the sometimes selectable integration time (µs to ms) and for cameras with thermal detectors the detector time constant itself (some ms) determine the camera response time. Accurate temperature values and time dependent temperature changes for transient heat processes can only be measured if the response time of the camera is much smaller than the time constant of the microsystem. Therefore cameras equipped with bolometer FPA are suitable only to a limited extent for thermal microsystem investigation.
Very accurate temperature measurements by radiation thermometry require an accurate knowledge of the object emissivity. Emissivity determination at microsystems is a complex problem.
Microsystems are made from a large variety of materials which are commonly not well suited for thermal imaging due to the emissivity properties of e.g. highly reflecting materials (metals), semitransparent materials (glass or silicon) or selectively emitting materials (plastics). The surface modification by additional colors or emissivity strips as used in standard thermal imaging applications fails because this would modify the physical properties of the microsystems dramatically. If the determination of absolute temperature values is necessary the emissivity can be determined by tempering the microsystem to known temperature using a climatic exposure test cabinet. The emissivity adjustment at the camera is changed to measure the known object temperature. The object emissivity is given by the correct emissivity adjustment at the camera. The emissivity can also be estimated by infrared spectroscopic measurements using an IR microscope [4].

Selected examples for IR imaging of Microsystems

- **Microfluidic systems – microreactors**

Silicon is the best known and best mastered material in microtechnology. The large mechanical strength, excellent thermal properties connected with a high temperature and a good chemical stability of silicon combined with the well established silicon micromachining technologies offer excellent possibilities to fabricate microreactors. Such reactors are suitable for chemical reactions at elevated temperatures and pressures.
Silicon is non absorbing in the MW region and is characterized by a flat wavelength dependence of the transmission at about 50%. In the LW region absorption features influence the transmission. But for the typical thickness of a silicon wafer ($\leq$ 1mm) the transmission is decreased by only 10 %. Therefore temperatures of the chemical reactants inside silicon microreactors can be analyzed by either MW or LW IR-cameras.
The silicon miroreactor shown in Fig. 4 was developed for process controlled strong exothermic liquid/liquid chemical reactions within 9 parallel microchannels (channel width approx. 300 µm). The special geometry and the configuration were designed using computer simulations to allow optimum mixing of the reactants.

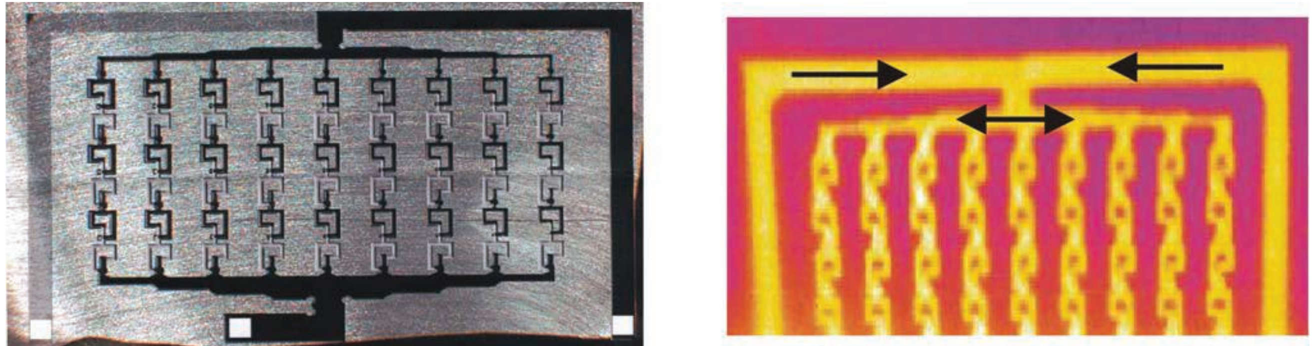

Fig. 4: Cutaway view of the Si-microreactor and IR-image of the reaction channels filled with hot water (flow directions marked by arrows)

The silicon microreactor was tested, e.g., for the nitration of diethyl urea with N_2O_5. The thermal imaging of this reaction resulted in an unexpected surprise. In contrast to expectations, inhomogeneous reactions occurred with hot spots along the reaction channels (see Fig. 5). Dependent on the pressure, the flow-rates and the temperature of the reactants within the reaction zone the IR-images show time dependent localized hot spots like “thunderbolds” in different reaction channels.
So far, the reasons for these results are unknown. Obviously, Fig. 5 is, however, a good example to show that time and spatially resolved temperature distributions are extremely valuable tools for reactor characterization and optimization. The thermal imaging results led to a complete redesign of the structures and the geometries in order to get a homogeneous and continuous distribution of the chemical reaction across the whole reactor.

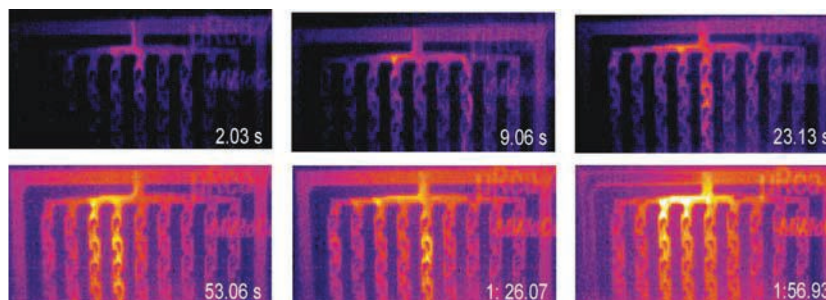

Fig. 5: Thermal imaging of a nitration reaction of urea in silicon microreactor, recorded with THV 550 MW camera. The numbers indicate the elapsed time after start of the reaction.

- **Miniaturized IR emitters**

New micro-machined thermal infrared emitters in TO-39 housing with protective cap, reflector, or IR transparent window are available for compact IR spectroscopy applications and non-dispersive infrared gas analysis (NDIR) [5]. Typical emitter areas are in the range of several mm^2. Fig. 6 depicts two types of miniaturized IR emitters. The miniaturized emitters consist of a resistive heating element on top of a thin insulating membrane suspended by a micro-machined silicon substrate. Due to the low thermal mass of the MEMS structure (heated membrane with a thickness in the µm-range) these emitters exhibit a time constant in the ms-range. The maximum emitter temperature amounts up to 750°C. The emitters are characterized by wavelength independent large emissivity values (typical 0.95 in the 2 – 14 µm range), low electrical power consumption, high electrical to infrared radiation output efficiency, an excellent long term stability and reproducibility. One of the most important benefits of these emitters is the possibility of fast electrical modulation with high modulation depth (typical 80% at 10 Hz), i.e. a chopper wheel for radiation modulation is no longer needed.

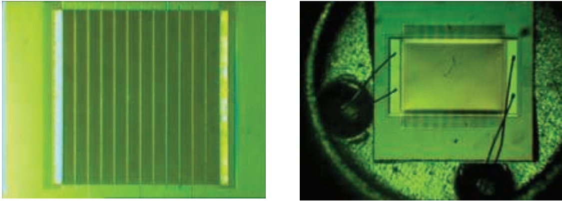

Fig. 6: Visible microscope images of two types of commercial miniaturized emitters
Type 1, left: Maximum temperature 450 °C, emitter area 2.1 x 1.8 mm^2
Type 2, right: Maximum temperature 750 °C, emitter area 2.8 x 1.8 mm^2

Using microscopic and high-speed thermal imaging during emitter operation the time constant as well as the temperature distribution can be analyzed as shown in Fig. 7 and Fig. 8, respectively. The spatial temperature distribution does have an influence on the angular dependence of the emitted radiation.
The radiance measurements indicate a spatially varying temperature distribution across the emitting area. This behavior is caused by the construction of the miniaturized emitter. The heated area is placed on a membrane area that is connected to the silicon substrate at its border. So the heat generated in the element is transported by thermal conduction to these borders via the membrane material. Due to the large thermal conductance of the bulk silicon the temperature at the borders will not increase during heating the membrane. The maximum temperature is achieved at the center of the membrane. The IR image of the type 1 emitter exhibits additional lines with reduced radiance, see Fig. 7 c (left). These lines are also visible in the microscopic image, see Fig. 7, they are the contact lines for current supply to the emitter. Due to the metal used for establishing these contact lines the emissivity and therefore the emitted radiance is reduced.
A time constant of τ = 32 ms is determined from the measurement of the temperature signal of the emitter surface temperature during voltage pulsed operation of the IR-emitter, see Fig. 8. The emitter represents a low frequency pass and can be characterized by the frequency f = 5 Hz for a $\omega\tau$ = 1 operation.

Emitter Type 1 Emitter Type 2

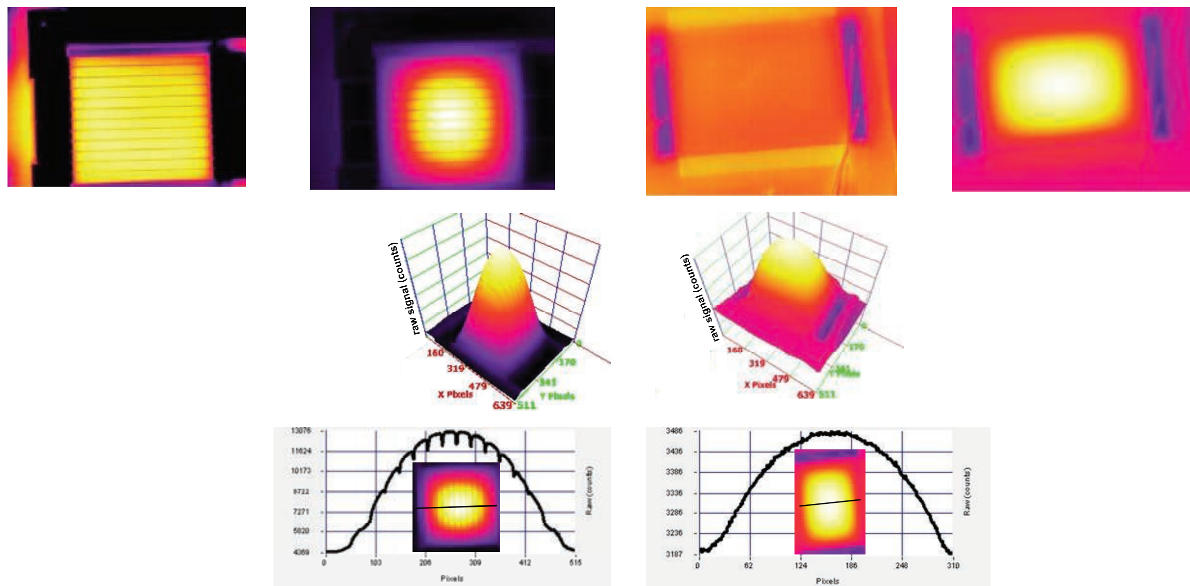

Fig. 7: Stationary spatial radiance distribution at the emitter surfaces (type 1 left, type 2 right)
top row: Thermal images of the emitter surface (stationary temperature distribution) without (left) and with applied voltage (right)
middle row: 3D-plot of the measured raw data signal distribution on the emitter surface with applied voltage
bottom row: Line profile of the measured raw data for applied voltage

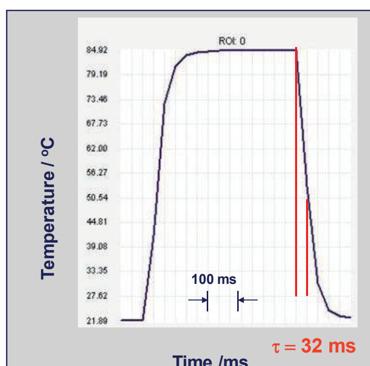

Fig. 8: Determination of the time constant from the transient temperature signal of the emitter surface temperature for the emitter type 1 after a 250 ms square wave electrical pulse (measurement at 600 Hz frame rate and 0.8 ms integration time, spot temperature measurement at the center of the emitter surface).

- **Thermal IR sensors – thermopiles and bolometers**

Microbolometers are very important components of the infrared imaging industry. The excellent achievable detector performance of microbolometers can not only be used for IR thermal imaging but also for other applications as well e.g. for non dispersive gas detection (NDIR), pyrometry or IR spectroscopy applications. Therefore a technology for single micromachined microbolometers and measurement techniques for characterizing the bolometer performance including microthermography have been developed [4]. A single bolometer consists of a thin layer of a material with a high temperature coefficient of resistivity (TCR) with electric contacts. The layer is thermally insulated from the surroundings. Fig. 9 depicts the lay-out of a single microbolometer.

A bulk micromachining technology based on anisotropic silicon etching was used [4]. First a silicon substrate was covered with a thin Si_3N_4 layer forming the membrane for the bolometer structure. A new bolometer material with a high TCR of – 2.5 … -3 %/K was developed. For perfect convertion of the incident radiation to heat an absorbing layer structure (maximum absorbance 0.95, adjustable wavelength for maximum absorbance within 2 -14 µm) was evaporated on top of the sensor area. Finally an inverse pyramid shape cavity of 500 µm x 500 µm is etched into the silicon substrate. KOH is a wet etch which attacks silicon preferentially in the (100) plane, producing a characteristic V-etch, with sidewalls [(111) –planes] that form a 54.7^{o} angle with the surface [6, 7]. The bolometers are thermally insulated from the silicon substrate by the supporting legs which simultaneously act as electric contacts. The pixel pitches are 100 µm and 250 µm. Fig. 9 bottom depicts a microscopic image of the bolometer after complete technological process (left) and the bolometer in a TO-housing (right). The packaging can be completed by mounting of a transistor cap with an infrared transparent window.

The heat capacitance C_{th} and the heat conductance G_{th} of the bolometer structure are important parameters for the bolometer performance [8]. Therefore the thermal design of the microbolometer structure has a strong influence on the detector performance. The voltage responsivity depends reciprocally on G_{th} and the time constant of the sensor equals the ratio of C_{th} and G_{th}.

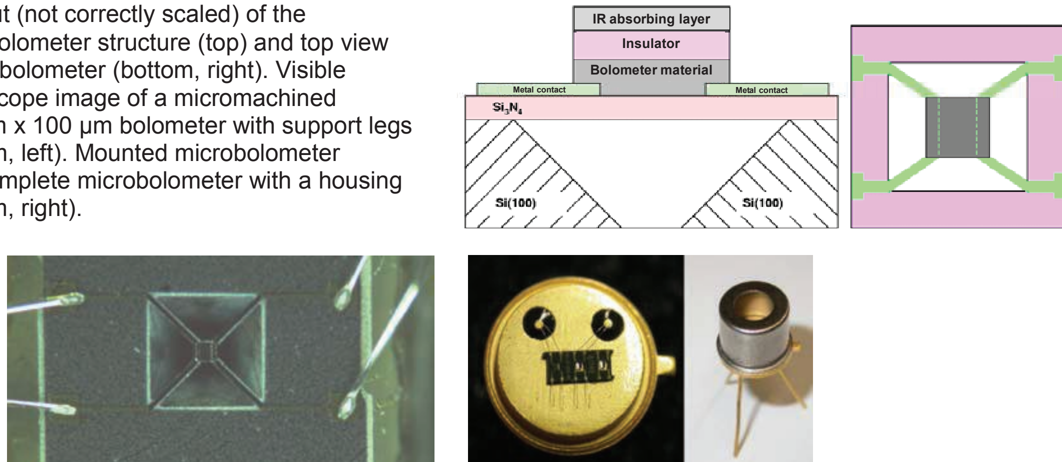

Fig. 9: Lay-out (not correctly scaled) of the microbolometer structure (top) and top view on the bolometer (bottom, right). Visible microscope image of a micromachined 100 µm x 100 µm bolometer with support legs (bottom, left). Mounted microbolometer and complete microbolometer with a housing (bottom, right).

Within the lay-out process a detailed thermal analysis of the structures was done. In order to compare the results of the numerical simulation with the parameters characterizing the processed bolometer structures and for further improvement of the detector performance the two values C_{th} and G_{th} have to be determined separately. Usually these two parameters are experimentally determined from time constant and sensitivity measurements. In order to increase the accuracy of the determination of these two parameters an electrical measurement combined with micro-thermography has been developed utilizing the self heating process of the bolometer if a voltage is applied [4]. Fig. 10 depicts the self heating effect of the bolometer by an applied voltage. The thermal conductance can be determined from the ratio of the electric power dissipated in the bolometer structure and the observed temperature change.

The temperature of the bolometer during this self heating process can be analyzed using microscopic thermal imaging for direct temperature determination or from the changed bolometer resistance with the known temperature dependent bolometer resistance. For the 100 x 100 μm^2 bolometer depicted in Fig. 10 a heat conductance of G_{th} = 4 µW/K was determined.

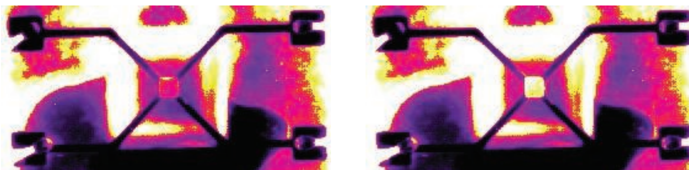

Fig. 10: IR image of a 100 µm x 100 µm microbolometer electrically heated by an applied voltage pulse (without voltage left, with applied voltage right)

With pulsed heating a time constant of about 4 ms of the microbolometer was determined from transient thermal imaging during the heating and cooling process, see Fig. 11. Similar to the analysis of the miniaturized emitters

different time constants for temperature rise and decay were found. The heat capacity was determined from the heat conductance G_{th} = 4 µW/K and the time constant $\tau \approx 4$ ms to be $C_{th} \approx 1.6 \cdot 10^{-8}$ J/K.
Furthermore the thermal images of the electrically self heated bolometer can be used to analyze the homogeneity of the temperature distribution on the bolometer area and the temperature drop due to thermal conductivity of the supporting legs of the bolometer. The IR image of the self heated bolometer in Fig. 12 allows to estimate the spatial sensitivity distribution. Lateral collecting effects increasing the effective detector area can be excluded. These results are confirmed by the results of a laser spot measurement, see Fig. 12.

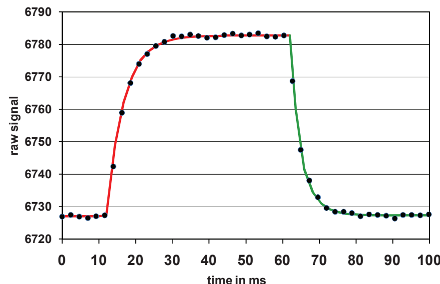

Fig. 11: Bolometer temperature rise and decay (measured as the raw data camera signal in the center of the bolometer area) during an applied 250 ms voltage pulse (FLIR SC6000 camera parameters: integration time 0.8 ms, frame rate 430 Hz). Approximation of the signal rise and decay by an exponential function with a time constant of 4.7 ms (red curve) and 3.4 ms (green curve), respectively.

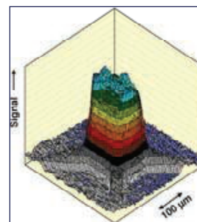

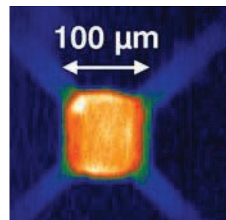

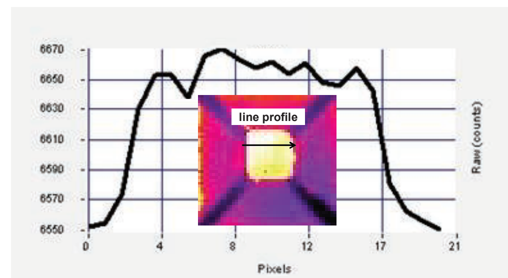

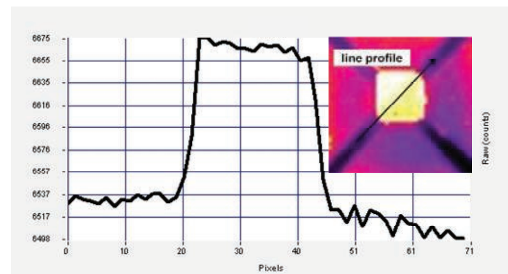

Fig. 12: Spatial sensitivity distribution determined by a laser spot measurement and thermal imaging of a 100 x 100 µm^2 bolometer.

top, left: 2 D – sensitivity distribution from a laser spot measurement.

bottom, left: False color representation of the spatial sensitivity distribution from the laser spot measurement.

right: Thermal image of the heated bolometer with raw signal line profile.

Summary

Microscopic and high speed thermography can a powerful tool in development and optimization of a lot of microsystems such as micro reactors, micro heat exchange systems, thermoelectric energy conversion systems, microactuators and microsensors.

References

[1] Möllmann, K.-P.; Lutz N.; Vollmer M., Wille, Ch; *Thermography of microsystems*; InfraMation 2004 Proceedings, Las Vegas, USA, Vol. 5, p. 183 – 195

[2] Möllmann, K.-P., F. Pinno, M. Vollmer; *Microscopic and high-speed thermal imaging: a powerful tool in physics R&D*; InfraMation 2009 Proceedings, Las Vegas, USA, Vol. 10, p. 303 – 318

[3] M. Vollmer, K.-P. Möllmann; *Infrared thermal imaging - fundamentals, research and applications*, Wiley-VCH (2010)

[4] Möllmann, K.-P; Trull, T.; Mientus, R.; *Single Microbolometer as IR Radiation Sensors - Results of a Technolgy Development Project*; Temperatur 2009; 24./25.06.2009; Berlin; Germany

[5] www.leister.com/axetris/

[6] G. Gerlach, W. Doetzel; *Introduction to Microsystem Technology*; Wiley-VCH (2008)

[7] Madou, M.; *Fundamentals of microfabrication*; CRC Press Boca Raton London New York Washington, D.C., 1997

[8] Hudson, R. D., Hudson, J. W. (Eds.); *Infrared Detectors*; Dowden, Hutchinson, and Ross, Wiley (1975)